Author/s:
Inbar, A;Nyman, P;Rengers, FK;Lane, PNJ;Sheridan, GJ

Title:
Climate Dictates Magnitude of Asymmetry in Soil Depth and Hillslope Gradient

Date:
2018-07-16

Citation:
Inbar, A., Nyman, P., Rengers, F. K., Lane, P. N. J. & Sheridan, G. J. (2018). Climate Dictates Magnitude of Asymmetry in Soil Depth and Hillslope Gradient. Geophysical Research Letters, 45 (13), pp.6514-6522. https://doi.org/10.1029/2018GL077629.

Persistent Link:
https://hdl.handle.net/11343/284254

Inbar Assaf (Orcid ID: 0000-0001-5861-963X)
Nyman Petter (Orcid ID: 0000-0002-0366-5548)
Rengers Francis, Kevin (Orcid ID: 0000-0002-1825-0943)
Lane Patrick, Norman (Orcid ID: 0000-0001-6121-8386)
sheridan Gary, james (Orcid ID: 0000-0003-1755-7334)

Climate dictates magnitude of asymmetry in soil depth and hillslope gradient

Assaf Inbar[1*], Petter Nyman[1], Francis K. Rengers[2], Patrick N. J. Lane[1], and Gary J. Sheridan[1]

[1]School of Ecosystems and Forest Sciences, Faculty of Science, University of Melbourne, Baldwin Spencer Building, Parkville, 3010, Victoria, Australia

[2]U.S. Geological Survey, Golden, Colorado, USA

[*]Corresponding author: Assaf Inbar (asinbar@gmail.com)

Key Points:

- In southeastern Australia we observe variations in the magnitude of n-s asymmetry across a climate gradient
- Soils were deeper and slopes steeper on polar-facing hillslopes
- Asymmetry peaked at a transition between water and energy limitations suggesting a long-term effect of vegetation on landscape evolution

This is the author manuscript accepted for publication and has undergone full peer review but has not been through the copyediting, typesetting, pagination and proofreading process, which may lead to differences between this version and the Version of Record. Please cite this article as doi: 10.1029/2018GL077629

Abstract

Hillslope asymmetry is often attributed to differential eco-hydro-geomorphic processes resulting from aspect-related differences in insolation. At mid-latitudes, polar facing hillslopes are steeper, wetter, have denser vegetation, and deeper soils than their equatorial facing counterparts. We propose that at regional scales, the magnitude in insolation-driven hillslope asymmetry is sensitive to variations in climate, and investigate the fire-prone landscapes in southeastern Australia to evaluate this hypothesis. Patterns of asymmetry in soil depth and landform were quantified using soil depth measurements and topographic analysis across a contemporary rainfall gradient. Results show that polar facing hillslopes are steeper, and have greater soil depth, than equatorial facing slopes. Furthermore, we show that the magnitude of this asymmetry varies systematically with aridity index, with a maximum at the transition between water and energy limitation, suggesting a possible long-term role of climate in hillslope development.

1 Introduction

The effect of hillslope aspect on vegetation (eg., Bale et al., 1998), soil (Anderson et al., 2013; Lybrand et al., 2011) and landform morphology (Gutiérrez-Jurado & Vivoni, 2013; Istanbulluoglu et al., 2008, Johnstone et al. 2017) is well recognized. In mid-latitudes polar facing (PF) hillslopes tend to be wetter and steeper than equatorial facing (EF) hillslopes (Poulos et al., 2012), which is attributed to differential eco-hydro-geomorphic processes across aspects (Istanbulluoglu et al., 2008) caused by different mean annual insolation (Pelletier et al., 2017; Yetemen et al., 2015) and associated vegetation patterns (eg., McGuire et al., 2014; Yetemen et al., 2015).

Vegetation reflects climatic conditions at large (eg., Budyko, 1974), intermediate (eg., Tesemma et al., 2014), and small (eg., Nyman et al., 2014) scales. Because vegetation cover has a strong effect on soil erosion (Istanbulluoglu et al., 2004; Istanbulluoglu & Bras, 2005) and development (eg., Amundson et al., 2015), local variations in microclimatic conditions often result in different soil depths (Goodfellow et al., 2014; Pelletier et al., 2013). At catchment

scales, these differences can result in soil depth asymmetry on opposing slopes (eg., Lybrand & Rasmussen, 2015; West et al., 2014). Over geologic timescales, the influence of vegetation cover could lead to asymmetric soil production, and/or erosion rates that would generate an asymmetric hillslope form (Pelletier et al., 2017).

Here we use the eastern uplands in SE Australia to study the effect of climate on soil depth and hillslope asymmetry. In this post-orogenic and fire-prone landscape, large differences in vegetation, flammability and fire regimes emerge from combinations of precipitation and topographically-driven differences in insolation (Nyman et al., 2015a). Studies in this region show that geomorphic processes, and in particular post-fire erosion and debris-flows, are sensitive to local variations in climatic forcings (Noske et al., 2016; Nyman et al., 2011, 2015b; Sheridan et al., 2016).

Given these known biotic and sediment transport asymmetries in the uplands, we investigated whether the current landscape shows evidence of hillslope asymmetry corresponding to observed contemporary processes. Within our study area, we tested the following hypotheses: (1) wetter PF hillslopes are consistently steeper and have deeper soils than EF hillslopes; and (2) the magnitude of asymmetry in both soil depth and hillslope gradient varies with climate, reaching a maximum where vegetation and soil hydraulic properties are the most contrasting. We tested these hypotheses by quantifying patterns of asymmetry in both soil depth and hillslope gradient across an aridity gradient.

2 Methods

2.1 Regional description

The eastern uplands in Victoria (Figure 1a) form part of the Great Dividing Range, a belt of ridges, plateaus and corridors in SE Australia, with elevations ranging from 200 to 2000 m ASL (above sea level). The eastern uplands consist mainly of Paleozoic marine sedimentary (mudstone, shale and sandstone) rocks; with some regional igneous plutons (granite and

granodiorite). Uplift peaked in late Cenozoic, and is now limited to isostatic rebound (Czarnota et al., 2014; Wellman, 1987). Annual variability in rainfall is largely driven by Southern Annular Mode (SAM), El Niño-Southern Oscillation (ENSO) and positive Indian Ocean Dipole (pIOD) events. The climate is temperate with mild summers, and cool, wet winters (Stern et al., 2000). Mean annual precipitation (MAP) range from 600 to 2500 mm yr^{-1} and mean annual temperatures are 25.8^{o}C to 17.6^{o}C in summer and 13.4^{o}C and -1.1^{o}C in winter, for low and high elevations, respectively. There is no evidence of glaciation during the last glacial maxima (LGM; 17-13.5ka BP) in the study area. Pollen and sediment records show that during the LGM, most of the uplands were treeless and dominated by herbal alpine communities. Rainforest and tall open forest became more widespread as the climate became warmer and precipitation increased (~6ka BP; McKenzie, 1997, 2002). This also resulted in higher fire activity, with fire-tolerant sclerophyll species increasingly replacing fire intolerant rainforests (Lynch et al., 2007).

Contemporary vegetation varies across the eastern uplands, depending largely on water availability and fire frequency. In high rainfall zones (MAP>1200 mm yr^{-1}) fire frequency is low (>100 yr interval) (Cheal, 2010), and forests are dominated by stands of tall (>50m) *Eucalyptus regnans trees,* or by *E. Delegatensis* trees, when elevation is >1000 m ASL. By contrast, under drier conditions (MAP of 600-1000 mm yr^{-1}), fire frequency is significantly higher (<20-30 yr interval), and vegetation is dominated by dry open mixed-species forests with trees <30 m tall (e.g. *E.dives, E. macrorhyncha* and *E. polyanthemos*) and sparse understory. In intermediate rainfall zones (MAP 800-1200 mm yr^{-1}), vegetation structure is influenced by aspect. EF hillslopes are dominated by dry open-forest as described above, and PF hillslopes by a mixture of wet and damp open-forest structure consisting of *E. polyanthemos*, *E. radiata*, *E. globulus*, *E. cypellocarpa*, and *E. viminalis*. Erosion rates from undisturbed forest are generally low (<0.1 t ha^{-1}) but increase substantially after fire, particularly in the drier forest (eg., Noske et al., 2016), where soil hydraulic properties are more conducive to producing surface runoff (eg., Sheridan et al., 2016; Van der Sant et al., 2018). Soil hydraulic properties, vegetation structure and microclimate are all strongly related to Aridity Index (AI) which has been calculated at the

hillslope scale (20m resolution) from the ratio of mean annual potential evapotranspiration [mm yr^{-1}] to annual precipitation (Nyman et al., 2014).

2.2 Asymmetry Calculations

2.2.1 Quantifying soil depth asymmetry

Asymmetry in the eastern uplands was investigated with respect to AI using three focus-sites (Figure 1) located in the Norton Gully Sandstone (NGS) formation, which consists of variable (although mostly vertical) bedded strata of marine sedimentary rocks, that mainly include relatively thick strata of sandstone (with some siltstone and claystone layers). The three focus sites host a gradient of temperate forest types (as described above) referred to here as wet (MAP~1660 mm yr^{-1}), damp (MAP~1290 mm yr^{-1}) and dry (MAP~940 mm yr^{-1}), in accordance with the regional system for ecological vegetation classification (EVC; Cheal (2010)). These sites were used for in-depth analysis of soil and hillslope asymmetry. For the wet, damp and dry sites, the respective mean elevations are 811, 449 and 390m and mean annual temperature are 10^{o}C, 13^{o}C and 14^{o}C.

Soil depth was quantified by field measurements along contour lines on PF and EF hillslopes at each focus site (Figure 2). Depth measurements were obtained by hand auger, motorized auger, rod penetration apparatus (until refusal point), road cutting surveys (when available), and soil pits. Several trials were performed across different methods (usually near a soil pit or a roadcut) to ensure consistency. Depth measurements were replicated 1-4 times at each sampling point. Altogether, there were 111 sampling points. Sampling was limited to contributing areas < 0.01 km^2, thus ensuring that data represent planar hillslopes, and not convergent domains. This cut-off area was estimated by the mean area at the inflection point of the hillslope/colluvial hollow in the Slope-Area (S-A) plots (eg., Chadwick et al., 2013) (Figure 3).

Mean soil depth, $\overline{S_d}$, from each hillslope was used to calculate a soil depth asymmetry index (SAI) where: SAI $= \overline{S_{d_p}}/\overline{S_{d_e}}$, and $\overline{S_{d_p}}$ and $\overline{S_{d_e}}$ are mean soil depth [m] of the PF and EF hillslopes, respectively. SAI represents the direction and magnitude of the asymmetry in soil depth; SAI $= 1$ indicates no asymmetry, SAI >1 when soils on the PF slopes are deeper than those on the equatorial faces, and vice versa.

A continuous metric of expected SAI was estimated from a function describing the change in observed $\overline{S_d}$ with AI:

[Eqn. 1]
$$\overline{S_d} = \frac{1}{1 + \exp^{-4.8\,(AI-1.6)}} + 0.19$$

A sigmoid model represented the best fit to measured data (R^2=0.45 when using all data points; R^2=0.84 when using means at each site). From Eqn. 1, the expected SAI was calculated at regular intervals along the AI gradient from the estimated difference in soil depth on PF and EF slopes (see S1, Supporting Information).

2.2.2 Quantifying hillslope asymmetry

A regional analysis of hillslope asymmetry was performed using elevation data from the entire eastern uplands domain. Hillslope asymmetry index (HAI) was quantified using the same approach as the SAI, where HAI $= G_p/G_e$, and (G_p) and (G_e) are median gradient of PF and EF hillslopes, respectively. *HAI* was calculated for a sample of 81 5x5 km terrain patches (including terrain patches from the three focus sites) across the eastern uplands varying in geology and mean AI (Figure 1a). For each of these terrain patches, median gradient was calculated for PF and EF aspect bins using a 10m DEM (Supporting information S2). PF and EF aspect bins were defined to include aspect values of 90^o -270^o and 270^o-90^o, respectively. These terrain patches were sampled from the spectrum of AI categories using the criteria that the site: (i) must be mostly forested; (ii) must be mountainous and dissected; (iii) contains east-west trending ridges; and (iv) contain no escarpments. To constrain the analysis to hillslopes close to the ridgeline, all

pixels with slopes lower than 5^o and with areas higher than 0.1 km^2 were removed from the calculation.

Asymmetry was further examined using slope area (S-A) curves for north and south aspects in 5x5km terrain patches centered on the three focus sites (Figure 1). Slope and drainage area were calculated with a D8 approach using the Topotoolbox2 package (Schwanghart & Scherler, 2014) for MATLAB (MathWorks®, USA), where the ridge occupied the middle of the rectangular polygon to minimize edge effects. The S-A curves were created by plotting the median gradient within drainage area bins. S-A curves were used to determine geomorphically distinct process-zones (Istanbulluoglu et al., 2008; Yetemen et al., 2010).

3 Results

Mean soil depths ranged from 0.28-1.17 m and were strongly related to AI (Figure 2a). A nonlinear decrease in soil depth with AI ($0.9 < AI < 1.5$) results in a SAI values that peaks in the damp to dry domain (Figure 2b).

Values of HAI (Figure 2c) and the S-A curves (Figure 3) at the focus sites indicate that PF hillslopes are consistently steeper, but that topographic asymmetry is least developed at the wet site. The patterns of HAI at the focus sites are representative of HAI more broadly across the domain despite heterogeneity in local geology (Figure 2c). A regional-scale analysis across all 81 terrain patches showed that PF hillslopes were on average 8.6% steeper than EF ones, with a maximum of 15% difference in a transitional domain between wet (energy limited) and dry (water limited) conditions. Interestingly, HAI peaks between $1.5 < AI < 2$ after which it decreases to lower values (Figure 2c).

The S-A curves from the focus sites reveal distinct trends that change as a function of MAP and aspect (Figure 3). Median gradient increases with MAP with maximum of 0.4 and 0.6 for PF hillslopes at the dry and wet sites, respectively. Dry sites have shorter hillslopes and a more pronounced debris-flow dominated zone than wet and damp sites (Figure 3). PF slopes are

consistently steeper for a given contributing area than EF slopes, although this difference also diminishes at the wet site (Figure 3c).

4 Discussion

Studies had shown that PF hillslopes at low latitudes are usually steeper than EF hillslopes (Pelletier et al., 2013, 2017; Yetemen et al., 2010). Our results from the eastern uplands support these observations. This pattern has been ascribed to lower insolation, wetter conditions, denser vegetation and lower erodibility across PF hillslopes (Istanbulluoglu et al., 2008; Yetemen et al., 2010). The fact that asymmetry persists across a variety of geological structures, points to climate, and insolation in particular, as being the underlying cause (Pelletier & Swetnam, 2017; Poulos et al., 2012; Yetemen et al., 2015). In a study across the American cordillera, Poulos et al. (2012) found that the magnitude of hillslope asymmetry is sensitive to latitude, and that the direction of asymmetry reverses in high latitudes in both hemispheres. Our results show that in the eastern uplands, hillslope asymmetry is highly sensitive to aridity, and that variations in local climatic factors are of sufficient magnitude to produce regional-scale variability in magnitude of asymmetry, similar to observed continental-scale analyses (Pelletier et al., 2017; Poulos et al., 2012). Our data show that as MAP increases, the difference between the mean gradient for a given contributing area of the PF and EF hillslopes diminishes (Figure 3). Across all geological structures and a broad range of aridity, a "humped" pattern of HAI emerges with contemporary climate (Figure 2c), emphasizing the role of climate on landscape evolution, and that the effect of climate variability on hillslope processes is not equal across the domain.

Fingerprints of geomorphic processes that shape the landscape can be found in soil depth patterns. Our results show a threshold-type decrease in soil depth with AI (Figure 2a). This decrease occurs despite the pronounced reduction in hillslope gradient as climate becomes drier (Figure 3). This result is noteworthy and somewhat counterintuitive with respect to theoretical transport laws that dictate rates of hillslope diffusion (Dietrich et al., 2003), and points to a

nonlinear effect of climate on soil stability that tends to increase with vegetation cover (Istanbulluoglu et al. 2008). Other studies have found similar relationships between soil depth (Goodfellow et al., 2014) and other soil properties (Chadwick & Chorover, 2001; Slessarev et al., 2016) with aridity, pointing to differences in soil profile development processes across a specific band of climatic settings.

There is evidence that the observed pattern in soil depth (Figure 2a) may be caused by climatically-driven thresholds in vegetation, fire and soil hydraulic properties. Sheridan et al. (2016), for instance, found post-fire infiltration capacity in dry forests to be one order of magnitude lower than in wet forests. Similar differences in soil hydraulic properties were shown to lead to 2 orders of magnitude difference in runoff ratios according to a study by Van der Sant et al. (2018). Findings of systematic increases in surface runoff and erosion rates with AI (Noske et al., 2016; Van der Sant et al., 2018), and decreases in soil depth with AI (Figure 2a), suggest that fluvial erosion tends to dominate over gravity driven processes (e.g., bioturbation, creep, etc.) in soil transport and hillslope evolution under drier systems, and the opposite for wetter systems.

Thinner soils on EF hillslopes (Figure 2b), as found by previous studies (Johnstone et al., 2017; eg., Olyphant et al., 2016; West et al., 2014), point to higher erosion rates on these hillslopes than on PF ones. In addition to higher fire frequency (Cheal, 2010; Duff et al., 2018), local studies showed an increase in post-fire erosion with AI (Noske et al., 2016; Nyman et al., 2015b). The more pronounced debris flow domains in dry focus sites (Figure 3a) indicate that this type of erosion process operates with higher frequency than in wetter systems. This is consistent with analyses of contemporary erosion processes that show that the frequency of post-fire debris flows is higher on dry EF slopes (Nyman et al., 2015b).

Large differences in soil depth with AI will influence soil production and denudation. Heimsath et al. (1997) showed that it was possible to estimate soil production from measured erosion rates. Here we invert this approach and estimate long-term erosion rates from the

exponential soil production function reported in Heimsath et al. (1997). The soil depth data suggest that under current conditions erosion rates varies by a factor of 7.4 between the dry and wet end-members of the domain. This calculation assumes dynamic equilibrium, but the results seem reasonable given the large differences in fire frequency (Cheal, 2010) and soil hydraulic properties (Sheridan et al., 2016) between wet and dry forests. Thus, it appears that the effect of climate on forest type, fire frequency and soil hydraulic properties dictate erosion rates and patterns of asymmetry across the aridity gradient (Figure 2).

These results motivate a conceptual model (Figure 4) that explains patterns in soil depth, SAI and HAI (Figure 2), based on system properties. Values of LAI (as proxy for productivity and forest cover), fire frequency, and soil infiltration capacity can be generalized into three climatic domains: energy-limited, transition, and water limited. Energy- and water limited climatic domains are defined depending on water availability with respect to AI (with the transition around AI=1) similar to Budyko (1974), and are separated by the transition domain, which hosts a threshold in system properties, as illustrated in Figure 4. The conceptual model proposes that the climatically-driven variation in productivity, fire frequency and soil hydraulic properties (Figure 4a-4b) can explain the observed patterns of asymmetry (Figure 4d) by affecting potential (Figure 4c) and actual erosion rates (Noske et al., 2016; Nyman et al., 2015b; Sheridan et al., 2016; Van der Sant et al., 2018).

The conceptual model illustrates how forest cover, fire frequency (Figure 4a), runoff and erosion (Figure 4c and 4e) contribute to the climate-related variation in asymmetry. Within the transitional climatic domain, small variations in AI cause significant differences in forest cover, fire frequency, infiltration capacity and erosion between EF and PF hillslopes, resulting in the emergence of strong soil depth and hillslope asymmetry (Figure 4d). Conversely, within the energy limited domain, infiltration capacity is high enough and fire frequency is low enough to sufficiently diminish any erosion differences between the hillslopes, resulting in similarly deep soils, low SAI and low hillslope asymmetry (Figure 2c and 4d). Within the water limited domain, differences in forest cover between the aspects is lower due to the lower hillslope gradient

(Figure 3). Dry conditions result in low infiltration capacity, high flammability and high erosion potential on both EF and PF hillslopes, and thus low SAI and HAI (Figure 2c and 4d).

The fact that peaks in soil and hillslope asymmetry occur at similar AI (Figure 2b, 2c and 4d) might suggest that the contemporary hydro-geomorphic setting, which gives rise to current soil profiles, are representative of the conditions that evolved the landscape. However, the large climatic fluctuations during the Quaternary (Augustin et al., 2004) might have resulted in significant changes in sediment production and erosion rates (Marshall et al., 2015). Therefore, the current hillslope and soil depth patterns are also shaped by those unknown boundary conditions. While the exact mechanism for alignment in SAI and HAI with respect to AI may be unclear, one possible explanation might be that warmer and wetter interglacial conditions comparable to present day climate (Lynch et al., 2007), leave a stronger legacy on landscapes than colder and drier conditions which were typical to the study area during glacial maxima (Reeves et al., 2013). Using landscape evolution models combined with cosmogenic radionuclide dating would be obvious avenues for future research to determine the timescale needed to develop soil depth and gradient asymmetries in response to climate variability.

5 Conclusions

By using measurements of soil depth and analysis of digital elevation models, we investigated the hypotheses that i) PF hillslopes are steeper and have deeper soils than drier EF hillslopes, and ii) magnitude in insolation-driven hillslope asymmetry is sensitive to variations in aridity (AI). The results showed that soils were deeper, and hillslopes steeper on the PF hillslopes compared to EF hillslopes, and that the magnitude of asymmetry both in soil depth and hillslope gradient peaked at a transition between water and energy limited domains. In the dry domain, the shorter hillslopes, lower hillslope gradients, pronounced debris-flow domains in slope areas curves, and shallower soils support contemporary studies showing that erosion rates are higher towards the drier end of the aridity spectrum. With a conceptual model we show that the patterns in soil depth and hillslope asymmetry are a likely result of climatically-driven

thresholds in erosion processes, caused by feedbacks between vegetation, fire frequency and soil hydraulic properties. We propose that interglacial climatic conditions, similar to contemporary climate, were the most geomorphically significant to landscape evolution and the development of hillslope asymmetry across the eastern uplands.

Acknowledgments

This project was funded by the Victorian Department of Land Water and Planning (DELWP) Integrated Forest Ecosystem Research program and ARC Linkage Project (LP 150200654). Data are available in Supporting Information.

References

Amundson, R., Heimsath, A., Owen, J., Yoo, K., & Dietrich, W. E. (2015). Hillslope soils and vegetation. *Geomorphology*, *234*, 122–132. https://doi.org/https://doi.org/10.1016/j.geomorph.2014.12.031

Anderson, R. S., Anderson, S. P., & Tucker, G. E. (2013). Rock damage and regolith transport by frost: An example of climate modulation of the geomorphology of the critical zone. *Earth Surface Processes and Landforms*, *38*(3), 299–316. https://doi.org/10.1002/esp.3330

Augustin, L., Barbante, C., Barnes, P. R. F., Marc Barnola, J., Bigler, M., Castellano, E., et al. (2004). Eight glacial cycles from an Antarctic ice core. *Nature*, *429*(6992), 623–628. https://doi.org/10.1038/nature02599

AusCover. (2017). Australian woody vegetation cover. Retrieved from http://auscover.org.au/purl/landsat-persistent-green-2000-2010

Austin, J. M., Gallant, J., & Van Niel, T. (2013). Mean monthly radiation surfaces for Australia at 1 arc-second resolution. In J. Piantadosi, R. S. Anderssen, & J. Boland (Eds.),

MODSIM2013, 20th International Congress on Modelling and Simulation, Modelling and Simulation Society of Australia and New Zealand (pp. 2506–2512).

Bale, C. L., Williams, J. B., & Charley, J. L. (1998). The impact of aspect on forest structure and floristics in some Eastern Australian sites. *Forest Ecology and Management*, *110*, 363–377.

Budyko, M. I. (1974). *Climate and life*. San Diego, California: Academic Press.

Chadwick, O. A., & Chorover, J. (2001). The chemistry of pedogenic thresholds. *Geoderma*, *100*, 321–353. https://doi.org/https://doi.org/10.1016/S0016-7061(01)00027-1

Chadwick, O. A., Roering, J. J., Heimsath, A. M., Levick, S. R., Asner, G. P., & Khomo, L. (2013). Shaping post-orogenic landscapes by climate and chemical weathering. *Geology*, *41*(11), 1171–1174. https://doi.org/10.1130/G34721.1

Cheal, D. (2010). *Growth stages and tolerable fire intervals for Victoria's native vegetation data sets. Fire and Adaptive Management. Report No. 84*.

Czarnota, K., Roberts, G. G., White, N. J., & Fishwick, S. (2014). Spatial and temporal patterns of Australian dynamic topography from River Profile Modeling. *Journal of Geophysical Research: Solid Earth*, *119*(2), 1384–1424. https://doi.org/10.1002/2013JB010436

Dietrich, W. E., Bellugi, D. G., Sklar, L. S., Stock, J. D., Heimsath, A. M., & Roering, J. J. (2003). Geomorphic transport laws for predicting landscape form and dynamics. In P. R. Wilcock & R. Iverson (Eds.), *Prediction in geomorphology* (pp. 103–132). Florida, US: AGU.

Duff, T. J., Cawson, J. G., & Harris, S. (2018). Dryness thresholds for fire occurrence vary by forest type along an aridity gradient: evidence from Southern Australia. *Landscape Ecology*. https://doi.org/10.1007/s10980-018-0655-7

Goodfellow, B. W., Chadwick, O. A., & Hilley, G. E. (2014). Depth and character of rock weathering across a basaltic-hosted climosequence on Hawai‘i. *Earth Surface Processes and Landforms*, *39*(3), 381–398. https://doi.org/10.1002/esp.3505

Gutiérrez -Jurado, H. A., & V
controlled semiarid basin: I. Topographic analyses with high -resolution data sets.
Ecohydrology, *6*(1), 8–23. https://doi.org/10.1002/eco.280

Heimsath, A. M., Dietrich, W. E., Nishiizumi, K., & Finkel, R. C. (1997). The soil production function and landscape equilibrium. *Nature*, *388*(6640), 358–361. https://doi.org/10.1038/41056

Istanbulluoglu, E., & Bras, R. L. (2005). Vegetation-modulated landscape evolution: Effects of vegetation on landscape processes, drainage density, and topography. *Journal of Geophysical Research: Earth Surface*, *110*(2), 1–19. https://doi.org/10.1029/2004JF000249

Istanbulluoglu, E., Tarboton, D. G., Pack, R. T., & Luce, C. H. (2004). Modeling of the interactions between forest vegetation, disturbances, and sediment yields. *Journal of Geophysical Research: Earth Surface*, *109*, F01009. https://doi.org/0148-0227/04/2003JF000041$09.00

Istanbulluoglu, E., Yetemen, O., Vivoni, E. R., Gutiérrez-Jurado, H. A., & Bras, R. L. (2008). Eco-geomorphic implications of hillslope aspect: Inferences from analysis of landscape morphology in central New Mexico. *Geophysical Research Letters*, *35*(14), 1–6. https://doi.org/10.1029/2008GL034477

Johnstone, S. A., Finnegan, N. J., & Hilley, G. E. (2017). Weak bedrock allows north-south elongation of channels in semi-arid landscapes. *Earth and Planetary Science Letters*, *478*, 150–158. https://doi.org/10.1016/j.epsl.2017.08.037

Langhans, C., Lane, P. N. J., Nyman, P., Noske, P. J., Cawson, J. G., Oono, A., & Sheridan, G. J. (2016). Scale-dependency of effective hydraulic conductivity on fire-affected hillslopes. *Water Resources Research*, *52*(7), 5041–5055. https://doi.org/10.1002/2016WR018998

Lybrand, R., & Rasmussen, C. (2015). Quantifying climate and landscape position controls on soil development in semiarid ecosystems. *Soil Science Society of America Journal*, *79*(1), 104–116. https://doi.org/10.2136/sssaj2014.06.0242

Lybrand, R., Rasmussen, C., Jardine, A., Troch, P., & Chorover, J. (2011). The effects of climate and landscape position on chemical denudation and mineral transformation in the Santa Catalina mountain critical zone observatory. *Applied Geochemistry*, *26*, S80–S84. https://doi.org/10.1016/j.apgeochem.2011.03.036

Lynch, A. H., Beringer, J., Kershaw, P., Marshall, A., Mooney, S., Tapper, N., et al. (2007). Using the paleorecord to evaluate climate and fire interactions in Australia. *Annu. Rev. Earth Planet. Sci.*, *35*, 215–239. https://doi.org/https://doi.org/10.1146/annurev.earth.35.092006.145055

Marshall, J. A., Roering, J. J., Bartlein, P. J., Gavin, D. G., Granger, D. E., Rempel, A. W., et al. (2015). Frost for the trees: Did climate increase erosion in unglaciated landscapes during the late Pleistocene? *Science Advances*, *1*(10), e1500715. https://doi.org/10.1126/sciadv.1500715

McGuire, L. A., Pelletier, J. D., & Roering, J. J. (2014). Development of topographic asymmetry: Insights from dated cinder cones in the western United States. *Journal of Geophysical Research: Earth Surface*, *119*(8), 1725–1750. https://doi.org/10.1002/2014JF003081

McKenzie, G. M. (1997). The late Quaternary vegetation history of the south-central highlands of Victoria, Australia. I. Sites above 900 m. *Austral Ecology*, *22*(1), 19–36.

https://doi.org/10.1111/j.1442-9993.1997.tb00638.x

McKenzie, G. M. (2002). The late Quaternary vegetation history of the south-central highlands of Victoria, Australia. II. Sites below 900 m. *Austral Ecology*, *27*(1), 32–54. https://doi.org/10.1046/j.1442-9993.2002.01155.x

Montgomery, D. R., & Foufoula -Georgiou, E. (1
using digital elevation models. *Water Resources Research*, *29*(12), 3925–3934. https://doi.org/10.1029/93WR02463

Noske, P. J., Nyman, P., Lane, P. N. J., & Sheridan, G. J. (2016). Effects of aridity in controlling the magnitude of runoff and erosion after wildfire. *Water Resources Research*, *52*, 4338–4357. https://doi.org/10.1002/2015WR017611.Received

Nyman, P., Metzen, D., Noske, P. J., Lane, P. N. J., & Sheridan, G. J. (2015a). Quantifying the effects of topographic aspect on water content and temperature in fine surface fuel. *International Journal of Wildland Fire*, *24*(8), 1129–1142. https://doi.org/10.1071/WF14195

Nyman, P., Sheridan, G. J., Smith, H. G., & Lane, P. N. J. (2011). Evidence of debris flow occurrence after wildfire in upland catchments of south-east Australia. *Geomorphology*, *125*(3), 383–401. https://doi.org/10.1016/j.geomorph.2010.10.016

Nyman, P., Sherwin, C. B., Langhans, C., Sheridan, G. J., & Lane, P. N. J. (2014). Downscaling regional climate data to calculate the radiative index of dryness in complex terrain. *Australian Metrological and Oceanographic Journal*, *64*(2), 109–122. https://doi.org/10.22499/2.6402.003

Nyman, P., Smith, H. G., Sherwin, C. B., Langhans, C., Lane, P. N. J., & Sheridan, G. J. (2015b). Predicting sediment delivery from debris flows after wildfire. *Geomorphology*,

250, 173–186. https://doi.org/http://dx.doi.org/10.1016/j.geomorph.2015.08.023

Olyphant, J., Pelletier, J. D., & Johnson, R. (2016). Topographic correlations with soil and regolith thickness from shallow-seismic refraction constraints across upland hillslopes in the Valles Caldera, New Mexico. *Earth Surface Processes and Landforms*, *41*(12), 1684–1696. https://doi.org/10.1002/esp.3941

Pelletier, J. D., Barron-Gafford, G. A., Breshears, D. D., Brooks, P. D., Chorover, J., Durcik, M., et al. (2013). Coevolution of nonlinear trends in vegetation, soils, and topography with elevation and slope aspect: A case study in the sky islands of southern Arizona. *Journal of Geophysical Research:Earth Surface*, *118*(2), 741–758. https://doi.org/Doi 10.1002/Jgrf.20046

Pelletier, J. D., Barron-Gafford, G. A., Guttierez-Jurado, H., Hinckley, E.-L. S., Istanbulluoglu, E., McGuire, L. A., et al. (2017). Which way do you lean? Using slope aspect variations to understand Critical Zone processes and feedbacks. *Earth Surface Processes and Landforms*, *In press*. https://doi.org/10.1002/esp.4306

Pelletier, J. D., & Swetnam, T. L. (2017). Asymmetry of weathering-limited hillslopes: The importance of diurnal covariation in solar insolation and temperature. *Earth Surface Processes and Landforms*, *42*(9), 1408–1418. https://doi.org/10.1002/esp.4136

Poulos, M. J., Pierce, J. L., Flores, A. N., & Benner, S. G. (2012). Hillslope asymmetry maps reveal widespread, multi-scale organization. *Geophysical Research Letters*, *39*(6). https://doi.org/10.1029/2012gl051283

Rees, D. B. (1982). *A study of soils in the Reefton experimental area; with particular reference to hydrological properties*. Melbourne.

Reeves, J., Barrows, T. T., Cohen, T., Kiem, A., Bostock, H., Fitzsimmons, K., et al. (2013).

Climate variability over the last 35,000 years recorded in marine and terrestrial archives in the Australian region: an OZ-INTIMATE compilation. *Quaternary Science Reviews*, *74*, 21–34. https://doi.org/https://doi.org/10.1016/j.quascirev.2013.01.001

Schwanghart, W., & Scherler, D. (2014). Short Communication: TopoToolbox 2–MATLAB-based software for topographic analysis and modeling in Earth surface sciences. *Earth Surface Dynamics*, *2*(1), 1–7. https://doi.org/10.5194/esurf-2-1-2014

Sheridan, G. J., Nyman, P., Langhans, C., Cawson, J., Noske, P. J., Oono, A., et al. (2016). Is aridity a high-order control on the hydro-geomorphic response of burned landscapes? *International Journal of Wildland Fire*, *25*(3), 262–267. https://doi.org/10.1071/WF14079

Slessarev, E. W., Lin, Y., Bingham, N. L., Johnson, J. E., Dai, Y., Schimel, J. P., & Chadwick, O. A. (2016). Water balance creates a threshold in soil pH at the global scale. *Nature*, *540*(7634), 567–569. https://doi.org/10.1038/nature20139

Stern, H., de Hoedt, G., & Ernst, J. (2000). Objective classification of Australian climates. *Australian Meteorological Magazine*, *49*(2), 87–96.

Stock, J. D., & Dietrich, W. E. (2003). Valley Incision by Debris Flows: Evidence of a Topographic Signature. *Water Resour. Res.*, *39*(4), 1089–1113. https://doi.org/10.1029/2001WR001057

Tesemma, Z. K., Wei, Y., Western, A. W., & Peel, M. C. (2014). Leaf area index variation for cropland, pasture and tree in response to climatic variation in the Goulburn-Broken catchment, Australia. *Journal of Hydrometeorology*, *15*, 1592–1606. https://doi.org/10.1175/JHM-D-13-0108.1

Van der Sant, R., Nyman, P., Noske, P. J., Langhans, C., Lane, P. N. J., & Sheridan, G. J. (2018). Quantifying relations between surface runoff and aridity after wildfire. *Earth Surface*

Processes and Landforms. https://doi.org/https://doi.org/10.1002/esp.4370

Wellman, P. (1987). Eastern highlands of Australia; their uplift and erosion. *Journal of Australian Geology & Geophysics*, *10*, 277–286.

West, N., Kirby, E., Bierman, P. R., & Clarke, B. A. (2014). Aspect-dependent variations in regolith creep revealed by meteoric 10Be. *Geology*, *42*(6), 507–510. https://doi.org/10.1130/G35357.1

Willgoose, G., Bras, R. L., & Rodriguez Iturbe, I. (1991). A physical explanation of an observed link area-slope relationship. *Water Resources Research*, *27*(7), 1697–1702. https://doi.org/10.1029/91WR00937

Yetemen, O., Istanbulluoglu, E., Flores -Cervantes, J. H., Ecohydrologic role of solar radiation on landscape evolution. *Water Resources Research*, *51*(2), 1127–1157. https://doi.org/doi:10.1002/2014WR016169

Yetemen, O., Istanbulluoglu, E., & Vivoni, E. R. (2010). The implications of geology, soils, and vegetation on landscape morphology: Inferences from semi-arid basins with complex vegetation patterns in Central New Mexico, USA. *Geomorphology*, *116*(3), 246–263. https://doi.org/10.1016/j.geomorph.2009.11.026

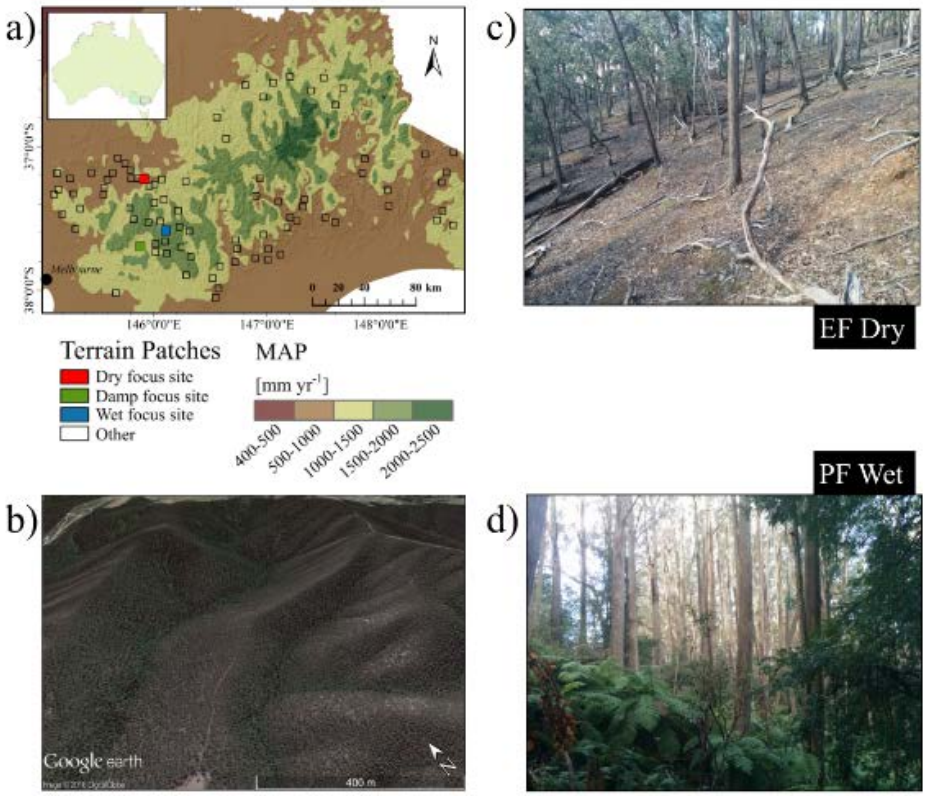

Figure 1. Map of the Eastern Uplands showing Mean Annual Precipitation (mm yr^{-1}). (a). Rectangular polygons are terrain patches that were used in the hillslope asymmetry index analysis (Figure 2c); Coloured polygons designate the three focus sites where S-A curves were compiled (Figure 3) and soil depth were measured (Figure 2a); (b) an example of hillslope asymmetry at a catchment near King Lake, Victoria (MAP 1000-1400 mm yr^{-1}; 37°31'48.39"S 145°18'51.30"E). Image by ©DigitalGlobe, 2018, Taken using Google Earth™; and example of forest structure at a dry EF hillslope (c) and wet PF hillslope (d). An example of the differences in vegetation structure between PF and EF hillslopes across wet, damp and dry focus sites are illustrated in Figure S3.

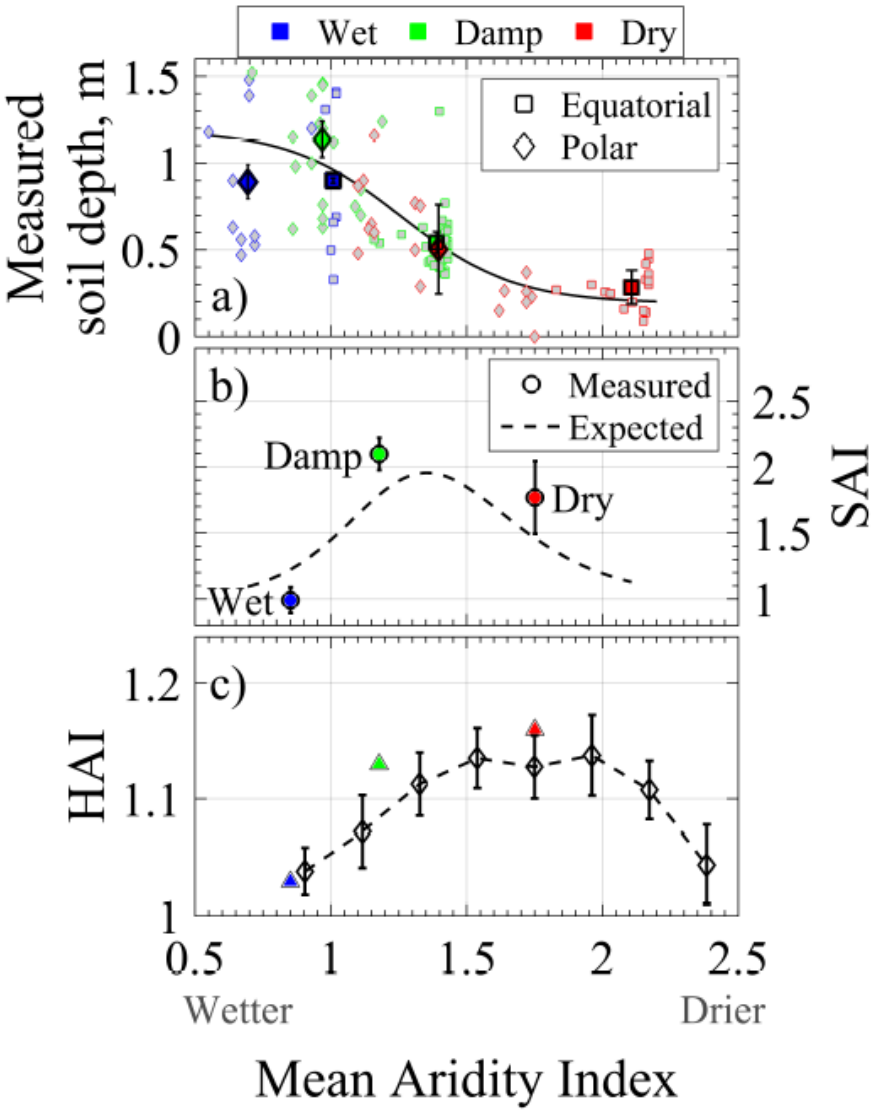

Figure 2. – (a) soil depth measurements and their means at the wet (blue), damp (green) and dry (red) focus sites as a function of mean AI (20m pixel resolution); (b) Soil depth asymmetry index (SAI) plotted against AI. Dashed line indicates the "expected" SAI across the domain (Supporting Information S1); and (c) Means of Hillslope Asymmetry Index (HAI) values for the

81 terrain patches (Figure 1a), binned by AI classes, and for the three focus sites. Bars represent standard deviation.

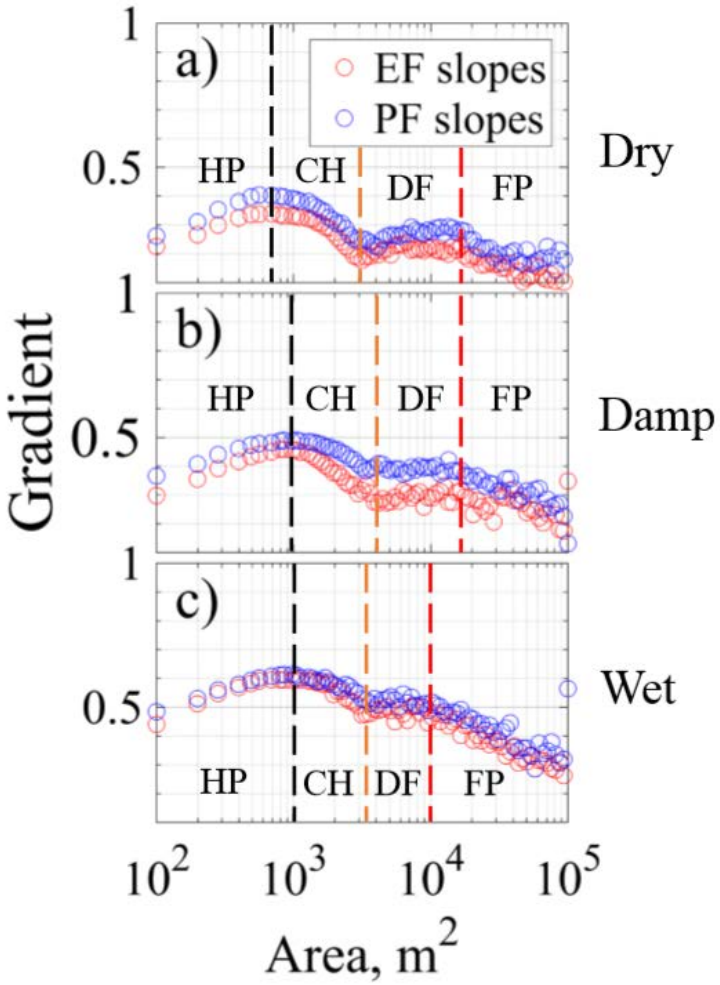

Figure 3. S-A curves from the dry (a), damp (b), and wet (c) focus sites. In this analysis two types of DEM sources were used (supporting information S2). Vertical lines (placed near inflection points) delineate portions of the landscape according to the following interpretation: hillslopes (HP) occupy low drainage areas which represents the area where diffusive processes dominate (Willgoose et al., 1991); High drainage areas, where the slope decrease as a power-law function, represent fluvial dominated portion of the landscape (FP) (Willgoose et al., 1991); The areas between the HP and FP represent portions of the landscape dominated by colluvial hollows

(CH) and debris-flow (DF) channels (e.g., Montgomery & Foufoula-Georgiou, 1993; Stock & Dietrich, 2003).

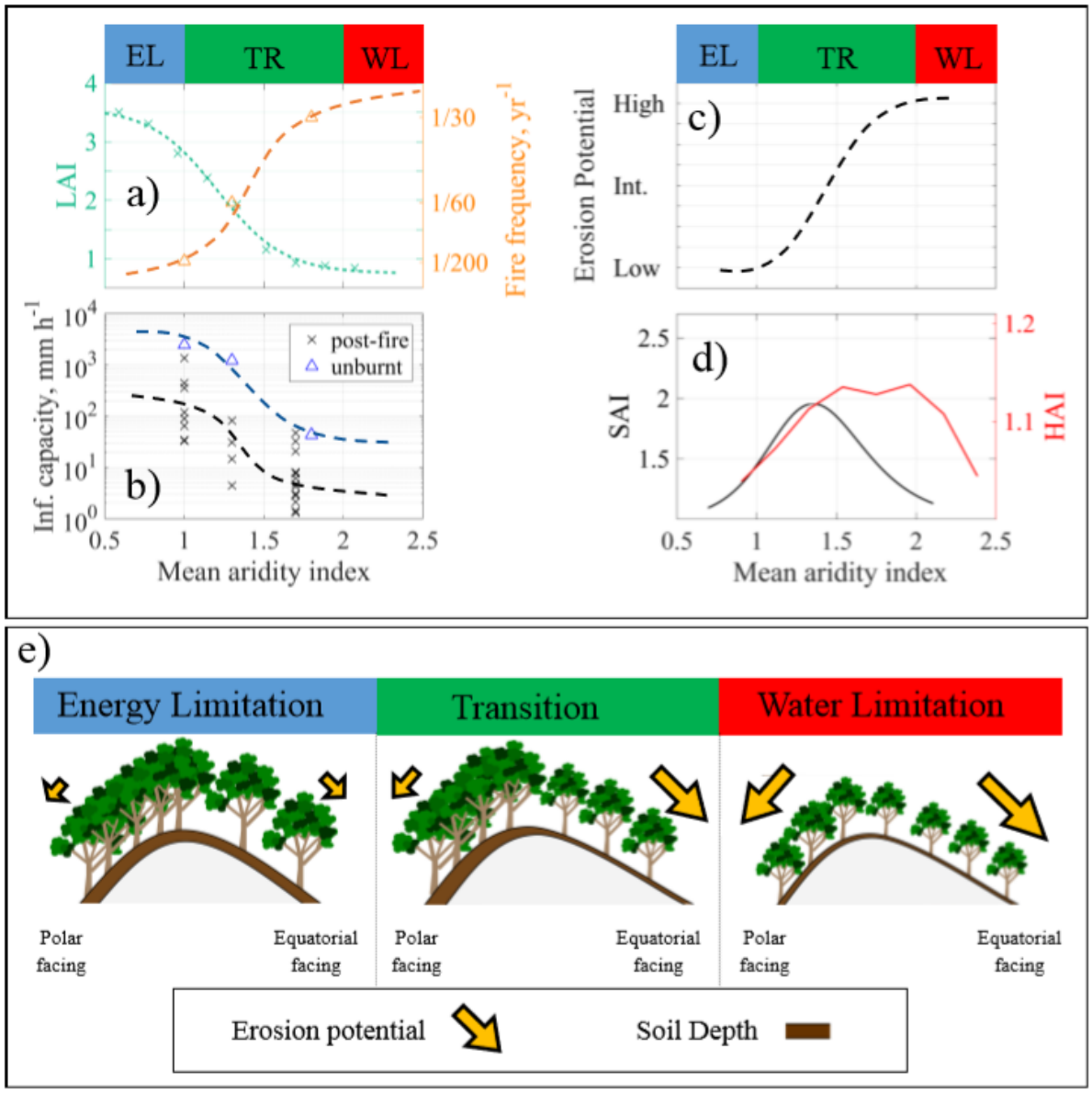

Figure 4. Conceptual model describing the development of patterns of soil and hillslope asymmetry. Remotely-sensed LAI, estimated fire frequency (a), measured background and post-fire infiltration capacity (b), estimated erosion potential (c) and SAI and HAI (d) are plotted as a function of aridity index. Schematic illustrations of hypothetical ridges, showing asymmetry in

vegetation structure, soil depth and hillslope gradient (e). Arrow sizes represent magnitude of erosion potential. Three climatic-domains are identified across the aridity index gradient (*sensu* Budyko (1974)): Energy limitation (EL), Water Limitation (WL) and the transition (TR). The conceptual model shows that patterns of SAI and HAI are dictated by climatically-driven thresholds in forest cover (LAI), fire frequency and soil hydraulic properties. Gridded LAI values for hillslopes across 5x5km polygons over the three focus sites were binned in regular intervals of aridity index (Nyman et al., 2014). LAI was calculated using (Austin et al., 2013): $LAI = -2\ ln(\ 1 - FPC)$, where FPC is Foliage Projective Cover product derived from an inter-annual time series of the green layer of Landsat fractional cover product (AusCover, 2017). Estimated fire frequency was calculated by averaging minimum and maximum Tolerable Fire Interval based on ecological vegetation classification (EVC, (Cheal, 2010)) representative of the focus sites. Infiltration capacity values were taken from *Langhans et al*. (2016), *Rees* (1982) and *Nyman et al*. (2011). Trend lines for both fire frequency and infiltration capacity are estimated based on the available data, and assuming minimum and maximum values at low and high aridity index values.